

Constraining Minimal $U(1)_{B-L}$ model from Dark Matter Observations

Tanushree Basak* and Tanmoy Mondal†

Theoretical Physics Division, Physical Research Laboratory, Ahmedabad 380009, India.

Abstract

We study the $B - L$ gauge extension of the Standard Model which contains a singlet scalar and three right-handed neutrinos. The vacuum expectation value of the singlet scalar breaks the $U(1)_{B-L}$ symmetry. Here the third generation right-handed neutrino is qualified as the dark matter candidate, as an artifact of Z_2 -charge assignment. Relic abundance of the dark matter is consistent with WMAP9 and PLANCK data, only near scalar resonances where dark matter mass is almost half of the scalar boson masses. Requiring correct relic abundance, we restrict the parameter space of the scalar mixing angle and mass of the heavy scalar boson of this model. Besides this, the maximum value of spin-independent scattering cross-section off nucleon is well-below the XENON100 and recent LUX exclusion limits and can be probed by future XENON1T experiment. In addition, we compute the annihilation of the dark matter into two photon final state in detail and compare with the Fermi-LAT upper bound on $\langle\sigma v\rangle_{\gamma\gamma}$ for NFW and Einasto profile.

arXiv:1308.0023v2 [hep-ph] 19 Feb 2014

*Electronic address: tanu@prl.res.in

†Electronic address: tanmoym@prl.res.in

1. INTRODUCTION

The existence of missing mass in the galaxies in the form of matter, namely ‘Dark matter’ (DM) was first proposed by Fritz Zwicky in the 1930s. According to the recent observations of the anisotropies in the cosmic microwave background by Wilkinson Microwave Anisotropy Probe (WMAP9) [1] – Universe consists of 71.4% of dark energy, 4.6% of luminous matter and 24% of DM. The DM content of the universe has even increased to 26.8% with the latest PLANCK results [2]. The most convincing evidence for dark matter on galactic scales comes from the observations of the galactic rotation curves [3] and bullet clusters [4]. The presence of dark matter is also supported by the weak gravitational lensing of distant galaxies by foreground structure [5] and the weak modulation of strong lensing around individual massive elliptical galaxies [6].

Unfortunately, the concept of dark matter does not find an explanation in the framework of the Standard Model (SM). Plenty of extensions of the SM were proposed with a motivation to introduce a suitable DM candidate. Among the plethora of candidates, the weakly interacting massive particles (WIMP) are the popular choice (for review see [7–9]). A simplest extension of the SM with a real or complex gauge singlet scalar field [10–14] (for latest update see [15]) has been extensively studied. The scalar turns out to be an appropriate DM candidate, which interacts only with the SM Higgs boson. Another possibility includes a renormalizable extension of the SM with a gauge singlet Dirac fermion (ψ) along with a gauge singlet scalar (S) [16–18], known as Singlet Fermionic Dark Matter (SFDM) model. In SFDM, the singlet scalar interact with the SM Higgs boson whereas ψ becomes the viable DM candidate, which interacts to the SM particles via S only. On the other hand, neutrino mass generation can be linked with DM mass through the radiative seesaw mechanism [19–21], and the Ma-model [22]. Among other possibilities, the minimal gauge extension of the SM with $U(1)_{B-L}$, and a discrete symmetry (Z_2 -parity) has been studied by several authors [19–21, 23–25] in the context of DM.

In this work, we study the minimal $U(1)_{B-L}$ extension of the SM [26–28], with an additional Z_2 -symmetry imposed on the model [23]. Here, only one of the right-handed (RH) neutrinos being odd under Z_2 -parity, serves as an excellent DM candidate. We obtain effectively a Higgs-portal DM which can annihilate into the SM particles (dominantly into W^+W^- and ZZ) and gives correct relic abundance [1, 2] near resonances where DM mass is almost half of the scalar boson masses. Our primary motivation is to restrict the choice of parameter space of this model, based on various recent experimental results of dark matter like relic abundance, limits on spin-independent scattering cross-section etc, which has not been considered in earlier studies. We emphasize that

the heavy scalar decay width depends strongly on the scalar mixing angle and hence plays a significant role in determining the relic density. Demanding correct relic abundance we constrain the parameter space of the scalar mixing angle and heavy scalar boson mass. We found that the spin-independent elastic scattering cross-section off nucleon is maximum at a particular value of scalar mixing angle and lies below the XENON100 [29, 30] and the latest LUX [31] exclusion limits. However the future XENON1T [32] experiment can further restrict the heavy scalar mass. Using the constraints on scalar mixing angle and heavy scalar mass, we have also calculated the annihilation cross-section into two photon final state ($\langle\sigma v\rangle_{\gamma\gamma}$) and finally compare with the upper bound on $\langle\sigma v\rangle_{\gamma\gamma}$ by Fermi-LAT [33] for different DM profiles. We observe that the resultant $\langle\sigma v\rangle_{\gamma\gamma}$ coincide with the Fermi-LAT data in the region where DM mass is almost half of the light scalar boson mass, otherwise it is well below the Fermi-LAT bound. Apart from DM phenomenology, neutrino mass can be generated in this model via Type-I seesaw mechanism. Here the lightest neutrino remains massless (because of odd- Z_2 parity of one of the RH-neutrinos), which is consistent with the observed oscillation data.

The paper is organized as follows: The next section contains a brief description of the model; we present an estimation of the relic density in Section 3; the direct detection of the DM has been investigated in Section 4; a detail calculation for annihilation into two photon final state can be found in Section. 5; finally we summarize our results and conclude in the last section. Appendix A shows the estimation of $w(s)$ required for the calculation of relic abundance. Appendix B contains the loop functions necessary for calculating the cross-sections $\langle\sigma v\rangle_{\gamma\gamma}$. A detail calculation of the total decay width of the heavy scalar boson has been shown in appendix C.

2. MODEL

In this work, we adopt the minimal $U(1)_{B-L}$ extension of the SM [26–28]. Along with the SM particles, this model contains: a SM singlet S with $B-L$ charge $+2$, three right-handed neutrinos $N_R^i (i = 1, 2, 3)$ having $B-L$ charge -1 . As this $U(1)_{B-L}$ symmetry is gauged, an extra gauge boson Z' is associated as a signature of the extended symmetry. Once the $B-L$ symmetry is broken spontaneously through the vacuum expectation value (vev) of S , this Z' becomes massive. Here, we also impose a Z_2 discrete symmetry. We assign Z_2 charge $+1$ (or even) for all the particles except N_R^3 [23]. This ensures the stability of N_R^3 which qualified as a viable DM candidate. The assignment of $B-L$ charge in this model eliminates the triangular $B-L$ gauge anomalies and ensures the gauge invariance of the theory.

Scalar Lagrangian of this model can be written as,

$$\mathcal{L}_s = (D^\mu \Phi)^\dagger D_\mu \Phi + (D^\mu S)^\dagger D_\mu S - V(\Phi, S), \quad (1)$$

where the potential term is,

$$V(\Phi, S) = m^2 \Phi^\dagger \Phi + \mu^2 |S|^2 + \lambda_1 (\Phi^\dagger \Phi)^2 + \lambda_2 |S|^4 + \lambda_3 \Phi^\dagger \Phi |S|^2, \quad (2)$$

with Φ and S as the Higgs doublet and singlet fields, respectively. After spontaneous symmetry breaking (SSB) the two scalar fields can be written as,

$$\Phi = \begin{pmatrix} 0 \\ \frac{v+\phi}{\sqrt{2}} \end{pmatrix}, \quad S = \frac{v_{B-L} + \phi'}{\sqrt{2}}, \quad (3)$$

with v and v_{B-L} real and positive. Minimization of eq. (2) gives

$$\begin{aligned} m^2 + 2\lambda_1 v^2 + \lambda_3 v v_{B-L}^2 &= 0, \\ \mu^2 + 4\lambda_2 v_{B-L}^2 + \lambda_3 v^2 v_{B-L} &= 0. \end{aligned} \quad (4)$$

To compute the scalar masses, we must expand the potential in eq. (2) around the minima in eq. (3). Using the minimization conditions, we have the following scalar mass matrix :

$$\mathcal{M} = \begin{pmatrix} \lambda_1 v^2 & \frac{\lambda_3 v_{B-L} v}{2} \\ \frac{\lambda_3 v_{B-L} v}{2} & \lambda_2 v_{B-L}^2 \end{pmatrix} = \begin{pmatrix} \mathcal{M}_{11} & \mathcal{M}_{12} \\ \mathcal{M}_{21} & \mathcal{M}_{22} \end{pmatrix}. \quad (5)$$

The expressions for the scalar mass eigenvalues ($m_H > m_h$) are:

$$m_{H,h}^2 = \frac{1}{2} \left[\mathcal{M}_{11} + \mathcal{M}_{22} \pm \sqrt{(\mathcal{M}_{11} - \mathcal{M}_{22})^2 + 4\mathcal{M}_{12}^2} \right]. \quad (6)$$

The mass eigenstates are linear combinations of ϕ and ϕ' , and written as

$$\begin{pmatrix} h \\ H \end{pmatrix} = \begin{pmatrix} \cos \alpha & -\sin \alpha \\ \sin \alpha & \cos \alpha \end{pmatrix} \begin{pmatrix} \phi \\ \phi' \end{pmatrix}, \quad (7)$$

where, h is the SM-like Higgs boson. The scalar mixing angle, α can be expressed as:

$$\tan(2\alpha) = \frac{2\mathcal{M}_{12}}{\mathcal{M}_{11} - \mathcal{M}_{22}} = \frac{\lambda_3 v_{B-L} v}{\lambda_1 v^2 - \lambda_2 v_{B-L}^2}. \quad (8)$$

Now we can calculate the quartic coupling constants by using eqs. (6,7 and 8).

$$\begin{aligned} \lambda_1 &= \frac{m_H^2}{4v^2}(1 - \cos 2\alpha) + \frac{m_h^2}{4v^2}(1 + \cos 2\alpha), \\ \lambda_2 &= \frac{m_h^2}{4v_{B-L}^2}(1 - \cos 2\alpha) + \frac{m_H^2}{4v_{B-L}^2}(1 + \cos 2\alpha), \\ \lambda_3 &= \sin 2\alpha \left(\frac{m_H^2 - m_h^2}{2v v_{B-L}} \right). \end{aligned} \quad (9)$$

In the presence of an extra $U(1)_{B-L}$ gauge theory the SM gauge kinetic terms is modified by

$$\mathcal{L}_{B-L}^{K.E} = -\frac{1}{4}F'^{\mu\nu}F'_{\mu\nu}, \quad (10)$$

where,

$$F'_{\mu\nu} = \partial_\mu B'_\nu - \partial_\nu B'_\mu. \quad (11)$$

The general covariant derivative in this model reads as

$$D_\mu \equiv \partial_\mu + ig_S T^\alpha G_\mu^\alpha + ig T^a W_\mu^a + ig_1 Y B_\mu + i(\tilde{g}Y + g_{B-L}Y_{B-L})B'_\mu. \quad (12)$$

Here, we consider only the ‘pure’ $B-L$ model, that is defined by the condition $\tilde{g} = 0$ at Electro-Weak (EW) scale. This implies zero mixing at tree level between Z' and Z bosons.

The relevant Yukawa coupling to generate neutrino masses is given by,

$$\mathcal{L}_{int} = \sum_{\beta=1}^3 \sum_{j=1}^2 y_\beta^j \bar{l}_\beta \tilde{\Phi} N_j - \sum_{i=1}^3 \frac{y_{n_i}}{2} \bar{N}_R^i S N_R^i \quad (13)$$

where, $\tilde{\Phi} = -i\tau_2 \Phi^*$.

The neutrino mass can be generated in this model via Type-I seesaw mechanism, where the mass matrices for light and heavy neutrino are given as,

$$m_{\nu_L} \simeq m_D^T m_M^{-1} m_D, \quad (14)$$

$$m_{\nu_H} \simeq m_M \quad (15)$$

where, $m_D = (y_\beta^j/\sqrt{2})v$, ($j = 1, 2$) and $m_{M_i} = -(y_{n_i}/\sqrt{2})v_{B-L}$, ($i = 1, 2, 3$).

Because of Z_2 -parity, N_R^3 has no Yukawa coupling with the left-handed lepton doublet, therefore the lightest neutrino remains massless. The masses of N_R^1 and N_R^2 are considered to be heavier than that of N_R^3 .

3. RELIC DENSITY

In the early universe when the temperature was high enough, the DM particles were in thermal equilibrium with the rest of the cosmic plasma and its number density had fallen off exponentially with temperature. But as temperature dropped down below the DM mass, the annihilation rate decreased and became smaller than the Hubble expansion rate. Then the DM species was decoupled from the cosmic plasma and number density experienced a “freeze-out” - hence we observe a significant relic abundance of DM today.

m_h	Γ_h	v_{B-L}	g_{B-L}
125 GeV	4.7×10^{-3} GeV	7 TeV	0.1

TABLE I: Choice of Parameters

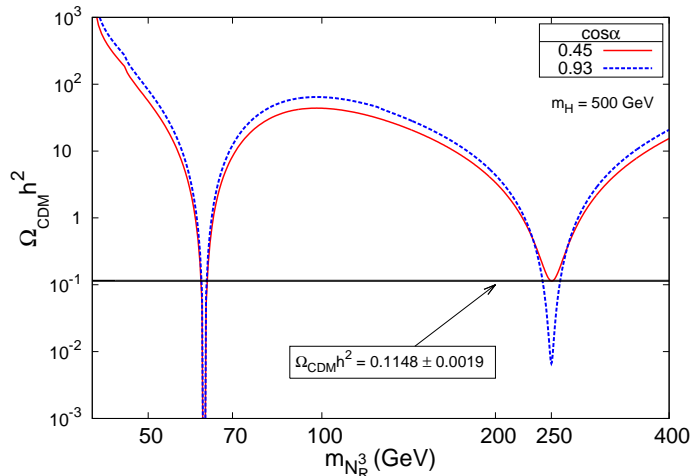


FIG. 1: Plot of relic abundance as a function of DM mass for $m_H = 500$ GeV with specific choices of scalar mixing angle $\cos \alpha = 0.935$ (blue-dashed), 0.45 (red-solid). The straight line shows the WMAP9 value, $\Omega_{CDM} h^2 = 0.1148 \pm 0.0019$.

In this model, the right-handed neutrino N_R^3 turns out to be a viable dark matter candidate as an artifact of the Z_2 charge assignment. We choose a specific set of benchmark values for (mass (m_h) and decay width (Γ_h) of SM-like Higgs boson, vev of singlet scalar S and $U(1)_{B-L}$ gauge coupling) our calculation, shown in Table.1, based on present experimental constraints [34]. However, the mass of the heavy scalar and the scalar mixing angle are not fixed.

The relic abundance of DM can be formulated as [35],

$$\Omega_{CDM} h^2 = 1.1 \times 10^9 \frac{x_f}{\sqrt{g^*} m_{Pl} \langle \sigma v \rangle_{ann}} \text{GeV}^{-1}, \quad (16)$$

where $x_f = m_{N_R^3}/T_D$ with T_D as decoupling temperature. m_{Pl} is Planck mass = 1.22×10^{19} GeV, and, g^* is effective number of relativistic degrees of freedom (we use, $g^* = 100$ and $x_f = (1/20)$). $\langle \sigma v \rangle_{ann}$ is the thermal averaged value of DM annihilation cross-section times relative velocity. DM interacts with the SM particles via Z' -boson and h, H . But, Z' -boson being heavy ($m_{Z'} \geq 2.33$ TeV [34]), the annihilation of DM into the SM particles takes place via h and H only. Thus, effectively we obtain a Higgs-portal DM model.

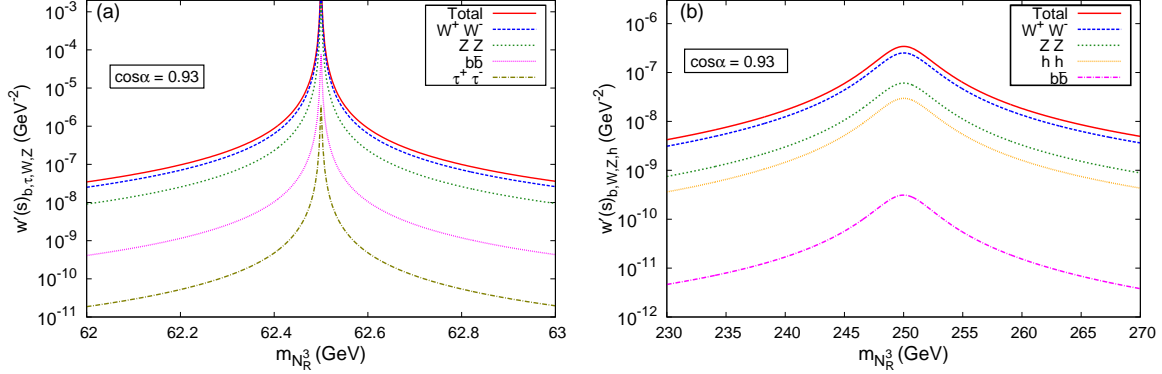


FIG. 2: Variation of $w'(s)$ near resonances : (a) $m_{N_R^3} = m_h/2$ and (b) $m_{N_R^3} = m_H/2$, with $m_h = 125$ GeV and $m_H = 500$ GeV, respectively.

$\langle\sigma v\rangle_{ann}$ can be obtained using the well known formula [36],

$$\langle\sigma v\rangle_{ann} = \frac{1}{m_{N_R^3}^2} \left\{ w(s) - \frac{3}{2} \left(2w(s) - 4m_{N_R^3}^2 w'(s) \right) \frac{1}{x_f} \right\} \Big|_{s=(2m_{N_R^3})^2}, \quad (17)$$

where prime denotes differentiation with respect to s (\sqrt{s} is the center of mass energy). Here, the function $w(s)$ (detail calculation in appendix A) depends on amplitude of different annihilation processes,

$$N_R^3 N_R^3 \longrightarrow b\bar{b}, \tau^+\tau^-, W^+W^-, ZZ, hh. \quad (18)$$

In Figure. 1 the relic density is plotted against DM mass for two specific choices (to be explained later in this section) of scalar mixing angles $\cos\alpha = 0.935, 0.45$ with $m_H = 500$ GeV. The straight line shows the latest 9-year WMAP data i.e, $\Omega_{CDM} h^2 = 0.1148 \pm 0.0019$ [1] (whereas latest PLANCK result is, $\Omega_{CDM} h^2 = 0.1199 \pm 0.0027$ at 68% CL [2]). The resultant relic abundance is found to be consistent with the reported value of WMAP-9 and PLANCK experiment only near resonance when, $m_{N_R^3} \sim (1/2) m_{h,H}$ ¹. The reason for the over abundance of DM except at the resonance can be understood in the following way : The annihilation cross-section of DM, being proportional to $y_{n_3}^2$ (where, $y_{n_3} = (\sqrt{2}m_{N_R^3})/v_{B-L}$), is heavily suppressed due to large value of v_{B-L} . Figure. 1 also exhibits a strong dependence on the mixing angle near the second resonance (i.e, $m_{N_R^3} \sim (1/2) m_H$). Since, the criterion for correct relic abundance is satisfied near scalar resonances, we have studied the contribution of different annihilation channels to the total annihilation cross-section in that region. We have plotted in Figure. 2 the variation of $w'(s)$ ($\langle\sigma v\rangle_{ann}$ depends on

¹ In principle, Z' resonance can also provide the correct relic abundance, but in that case the DM mass will be $\mathcal{O}(\text{TeV})$ (i.e $m_{N_R^3} \sim (1/2) m_{Z'}$), if we consider the current experimental bound on Z' mass [34].

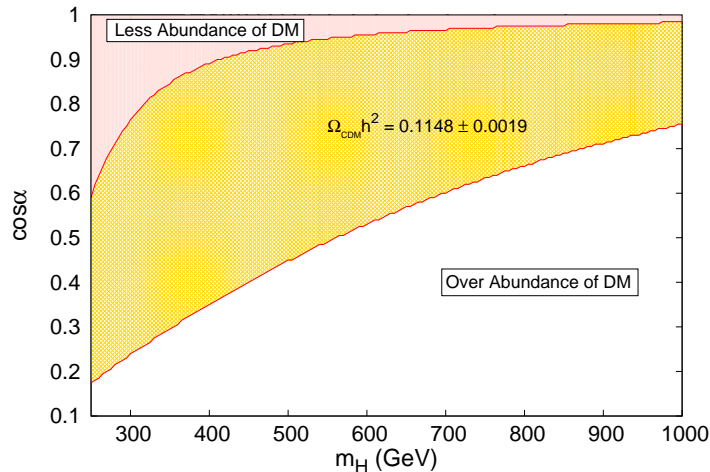


FIG. 3: Yellow region (in the middle) shows the allowed range of $\cos \alpha$ and m_H consistent with correct relic abundance as reported by WMAP9. The above-pink (below-white) region is disallowed due to under-abundance (over-abundance) of dark matter.

$w'(s)$ as shown in eq. (17)) near resonances $m_{N_R^3} = m_{h,H}/2$ for different annihilation channels like $b\bar{b}$, $\tau^+\tau^-$, W^+W^- , ZZ , hh . We observe that the dominant contribution to the total annihilation cross-section comes from the W^+W^- , ZZ (also final state hh dominance observed in Figure. 2(b)) final states, which is expected because of large SU(2) gauge coupling. In case of Figure. 2(a) a sharp (narrow) resonance peak is observed, whereas figure. 2(b) has a broad resonance due to larger decay width (Γ_H) of the heavy scalar, which also depends on scalar mixing angle (see appendix C).

Relic abundance near the second resonance depends on the following model parameters (unknown) : scalar mixing angle (α), heavy scalar mass (m_H) and decay width (Γ_H). But, these are not independent as Γ_H can be derived using $\cos \alpha$ and m_H . For large mixing angle, the total decay width of heavy scalar is large and hence the annihilation cross-section $\langle \sigma v \rangle_{ann}$ is less compared to that with minimal mixing scenario. This behavior is observed in Figure. 1, where $\Omega_{CDM} h^2$ is large for smaller value of $\cos \alpha$ (at $m_{N_R^3} \sim (1/2) m_H$) and vice-versa. We therefore perform a scan over the entire parameter range of m_H (300-1000 GeV) and $\cos \alpha$ to find the allowed region consistent with the 9-year WMAP data ($\Omega_{CDM} h^2 = 0.1148 \pm 0.0019$)[1]. In Figure. 3, the yellow region shows the allowed (by correct relic abundance) range of $\cos \alpha$ for different values of m_H , whereas the pink region is forbidden because the annihilation cross-section is enhanced for smaller mixing angle (smaller decay width Γ_H) leading to under-abundance of dark matter. On the other

hand, the white region is disallowed because of over-abundance.

4. SPIN-INDEPENDENT SCATTERING CROSS-SECTION

The effective Lagrangian describing the elastic scattering of the DM off a nucleon is given by,

$$L_{eff} = f_p \bar{N}_R^3 N_R^3 \bar{p} p + f_n \bar{N}_R^3 N_R^3 \bar{n} n , \quad (19)$$

where, $f_{p,n}$ is the hadronic matrix element, given by

$$f_{p,n} = \sum_{q=u,d,s} f_{Tq}^{(p,n)} a_q \frac{m_{p,n}}{m_q} + \frac{2}{27} f_{TG}^{(p,n)} \sum_{q=c,b,t} a_q \frac{m_{p,n}}{m_q}. \quad (20)$$

The f-values are given as in [37]

$$\begin{aligned} f_{Tu}^{(p)} &= 0.020 \pm 0.004, & f_{Td}^{(p)} &= 0.026 \pm 0.005, & f_{Ts}^{(p)} &= 0.118 \pm 0.062 , \\ f_{Tu}^{(n)} &= 0.014 \pm 0.003, & f_{Td}^{(n)} &= 0.036 \pm 0.008, & f_{Ts}^{(n)} &= 0.118 \pm 0.062 , \end{aligned}$$

and $f_{TG}^{(p,n)}$ is related to these values by

$$f_{TG}^{(p,n)} = 1 - \sum_{q=u,d,s} f_{Tq}^{(p,n)}. \quad (21)$$

Here, a_q is the effective coupling constant between the DM and the quark. We obtain the scattering cross-section (spin-independent) for the dark matter off a proton or neutron as,

$$\sigma_{p,n}^{SI} = \frac{4m_r^2}{\pi} f_{p,n}^2 \quad (22)$$

where, m_r is the reduced mass defined as, $1/m_r = 1/m_{N_R^3} + 1/m_{p,n}$.

An approximate form of a_q/m_q can be recast in the following form :

$$\frac{a_q}{m_q} = \frac{y_{n3}}{v\sqrt{2}} \left[\frac{1}{m_h^2} - \frac{1}{m_H^2} \right] \sin\alpha \cos\alpha , \quad (23)$$

where, $y_{n3} = \sqrt{2}m_{N_R^3}/v_{B-L}$ is the Yukawa coupling as specified in the second term of eq. (13).

From eq. (22), it is evident that, $\sigma_{p,n}^{SI} \propto (\sin 2\alpha)^2 f(m_H)$, which is maximum at $\alpha = \pi/4$ (or $\cos\alpha = 0.707$) irrespective of the choice of m_H . Therefore, the maximum value of $\sigma_{p,n}^{SI}$ increases as m_H is increased, which can be understood from eqs. (22, 23). Figure. 4 shows the maximum value of spin-independent scattering cross-section (i.e, with $\cos\alpha = 0.707$) of the DM off proton (σ_p^{SI}) for $m_H = 300$ GeV (green-dashed) and 900 GeV (black-solid) , whereas the blue and violet curves show the XENON100 (2012) [29, 30] and the latest LUX (at 95% C.L.) [31] exclusion plots,

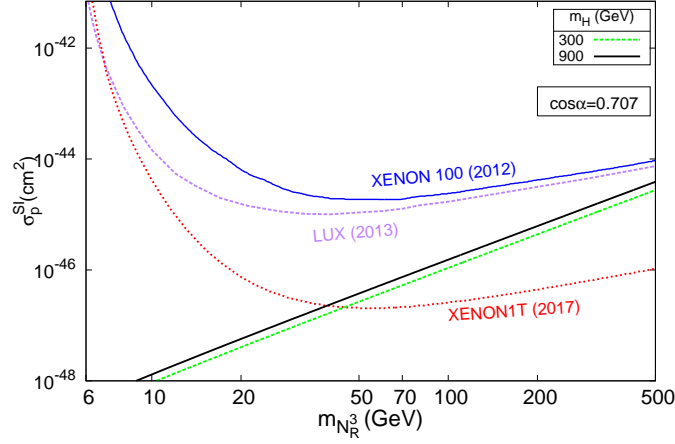


FIG. 4: Variation of σ_p^{SI} with $m_{N_R^3}$ for $m_H = 300$ GeV (green-dashed) and 900 GeV (black-solid) with $\cos \alpha = 0.707$. The blue and violet curves show the bound from XENON100 [29, 30] and LUX [31] data respectively. Red curve shows the projected limits for XENON1T [32].

respectively. The red-curve shows the projected limits on σ_p^{SI} for XENON1T experiment [32]. We observe that the value of the resultant cross-section with two different values of m_H for the entire range $6 \text{ GeV} \leq m_{N_R^3} \leq 500 \text{ GeV}$ lies much below the XENON100 and latest LUX exclusion limits. But, as the value of m_H is increased, the spin-independent cross-section becomes larger at higher values of DM mass and approaches the limits as reported by LUX and XENON100. As shown in Figure. 4, in future XENON1T data might severely restrict the choice of allowed m_H .

5. ANNIHILATION CROSS-SECTION INTO TWO PHOTONS

The RH-neutrino dark matter N_R^3 can also annihilate into two photon final state mediated by scalar bosons (h and H) through loop suppressed processes. Here, we consider mostly dominant contributions from top-quark and W-boson loops to this process [18].

The thermal averaging of the annihilation cross-section $\sigma v_{\gamma\gamma}$ can be obtained using [36]

$$\langle \sigma v \rangle_{\gamma\gamma} = \frac{1}{m_{N_R^3}^2} \left\{ w(s)_{\gamma\gamma} - \frac{3}{2} \left(2w(s)_{\gamma\gamma} - 4m_{N_R^3}^2 w'(s)_{\gamma\gamma} \right) \frac{1}{x_f} \right\} \Big|_{s=(2m_{N_R^3})^2}. \quad (24)$$

The function $w(s)_{\gamma\gamma}$ for massless final product is defined as,

$$w(s)_{\gamma\gamma} = \frac{1}{32\pi} \sum_{spins} |\mathcal{M}_{N_R^3 N_R^3 \rightarrow \gamma\gamma}|^2. \quad (25)$$

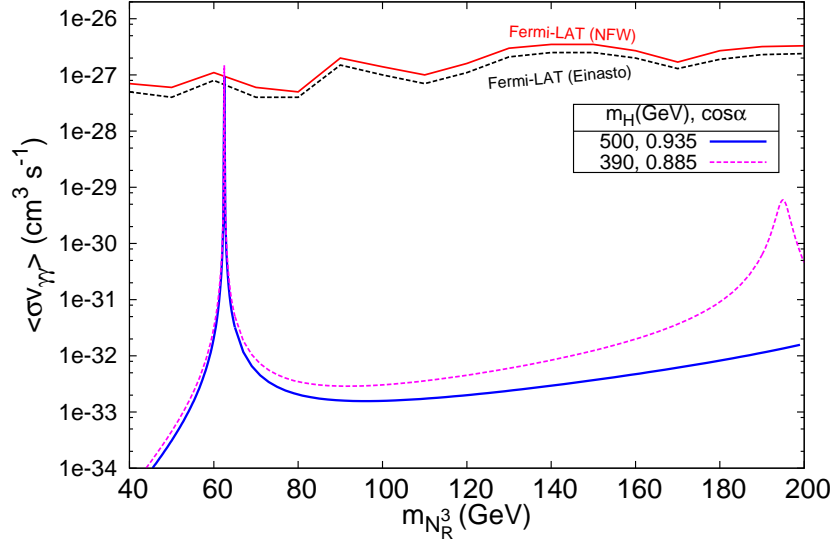


FIG. 5: Annihilation cross-section into two photon final state vs. dark matter mass with two specific choices : $\cos \alpha = 0.935, m_H = 500 \text{ GeV}$ (blue-solid) and $\cos \alpha = 0.885, m_H = 390 \text{ GeV}$ (purple-dashed) respectively. The upper-most two curves show the Fermi-LAT upper bound on $\langle \sigma v \rangle_{\gamma\gamma}$ [33] for NFW (solid-red) and Einasto (dashed-black) profile.

Taking into account contributions via h and H bosons we obtain,

$$\sum_{\text{spins}} |\mathcal{M}_{N_R^3 N_R^3 \rightarrow \gamma\gamma}|^2 = y_{n_3}^2 (s - 4m_{N_R^3}^2) \left\{ \frac{|\mathcal{M}_{h \rightarrow \gamma\gamma}|^2 \sin^2 \alpha}{(m_h^2 - s)^2 + m_h^2 \Gamma_h^2} + \frac{|\mathcal{M}_{H \rightarrow \gamma\gamma}|^2 \cos^2 \alpha}{(m_H^2 - s)^2 + m_H^2 \Gamma_H^2} \right. \\ \left. + \frac{|\mathcal{M}_{h \rightarrow \gamma\gamma}| |\mathcal{M}_{H \rightarrow \gamma\gamma}| \sin \alpha \cos \alpha \{ (m_h^2 - s)(m_H^2 - s) + m_h m_H \Gamma_h \Gamma_H \}}{((m_h^2 - s)^2 + m_h^2 \Gamma_h^2)((m_H^2 - s)^2 + m_H^2 \Gamma_H^2)} \right\}. \quad (26)$$

where, $\mathcal{M}_{h(H) \rightarrow \gamma\gamma}$ is the amplitude for the decay of $h(H)$ into two photons, which reads as [38, 39]

$$\mathcal{M}_{h(H) \rightarrow \gamma\gamma} = \frac{g_2 \alpha_{\text{em}} m_{h,H}^2}{8\pi m_W} \left[3 \left(\frac{2}{3} \right)^2 F_t(\tau_t) + F_W(\tau_W) \right] \cos \alpha (\sin \alpha), \quad (27)$$

where, $\tau_i = 4m_i^2/m_{h,H}^2$ ($i = W, t$) and $F_{W,t}(\tau_{W,t})$ are the loop functions for W -boson and top-quark respectively (see appendix B for detail calculation). α_{em} is the electromagnetic fine structure constant at the EW scale, $\alpha_{\text{em}}(m_Z) \sim 1/127$. $\text{SU}(2)$ gauge coupling is denoted as g_2 , whereas, m_W is the W -boson mass.

Figure. 5 shows the maximum annihilation cross-section into two photon final state as a function of dark matter mass with different values of $\cos \alpha$ and m_H . Here, we have chosen the maximum allowed value of $\cos \alpha$ corresponding to particular value of m_H as derived in Section. 3 (see Figure. 3). The blue(pink-dashed) curve shows the resultant $\langle \sigma v \rangle_{\gamma\gamma}$ for $\cos \alpha = 0.935(0.885)$ and $m_H = 500(390) \text{ GeV}$. It also shows a comparison with the Fermi-LAT upper bound on $\langle \sigma v \rangle_{\gamma\gamma}$

for Navarro-Frenk-White (NFW) (solid-red) and Einasto (dashed-black) profile [33]. We observe a clear coincidence between theoretical plots and Fermi-LAT data near resonance point where $m_{N_R^3} \sim (1/2) m_h$. A second peak is observed in the pink-curve due to a second resonance at $m_{N_R^3} \sim (1/2) m_H$ (i.e. at 195 GeV), but the maximum $\langle\sigma v\rangle_{\gamma\gamma}$ is found to be much below the exclusion limit of Fermi-LAT data. Last year, the analysis of Fermi-LAT data [40] had revealed a hint of a monochromatic gamma ray features [41–43] with $E_\gamma \simeq 130$ GeV coming from the vicinity of Galactic Center. One of the possible explanations of this phenomena could arise from the annihilation of DM with mass $129.8 \pm 2.4_{-13}^{+7}$ GeV and annihilation cross-section $\langle\sigma v\rangle_{\gamma\gamma} = (1.27 \pm 0.32_{-0.28}^{+0.18}) \times 10^{-27} \text{cm}^3 \text{sec}^{-1}$. It is possible to explain this monochromatic photon line in this model with a resonant heavy scalar near 260 GeV and achieve the desired cross-section. But, since the DM dominantly annihilates into W^+W^- , ZZ final states ($\langle\sigma v\rangle_{\gamma\gamma}$ is also suppressed as $\mathcal{O}(\alpha_{em}^2(M_Z))$), the continuum photon spectra supersaturate the monochromatic line-like feature.

6. SUMMARY AND CONCLUSION

We have studied a minimal $U(1)_{B-L}$ extended SM, where the third generation RH-neutrino becomes the plausible DM candidate by the virtue of an additional Z_2 -symmetry. The DM considered in this model is effectively Higgs-portal and annihilates dominantly into gauge boson (W^+W^- , ZZ) final states. We derive an important constraint on the allowed parameter space of the scalar mixing angle and heavy scalar mass in order to obtain correct relic abundance. Besides this, the relic abundance is found to be consistent with the recent WMAP9 and PLANCK data only near scalar resonances, i.e, $m_{N_R^3} = (1/2) m_{h,H}$. In future, PLANCK data can further restrict the choice of parameter space. The total annihilation cross-section is enhanced due to scalar resonance, otherwise it will be suppressed due to heavy Z' . The spin-independent elastic scattering cross-section of DM off a nucleon is maximum for $\cos \alpha = 0.707$, and hence maximum σ_p^{SI} depends on the value of heavy scalar mass. We observe that, σ_p^{SI} is well below the XENON100 and LUX exclusion limits for DM mass ranging from 5 – 500 GeV. But, future direct detection experiments like XENON1T can put stringent constraint on the choice of m_H . The annihilation cross-section of dark matter into $\gamma\gamma$ mediated by h and H bosons is compared with that of Fermi-LAT upper bound. We find an agreement between the theoretical plot and the Fermi-LAT data near scalar resonance where, $m_{N_R^3} = (1/2) m_h$. Although the required $\langle\sigma v_{\gamma\gamma}\rangle$ for explaining 130 GeV Fermi-line can be obtained in this model, but the gamma-ray continuum spectra produced due to W^+W^- , ZZ final state supersaturate this monochromatic line feature. In addition, this model can successfully

account for the neutrino masses generated via Type-I seesaw mechanism. In future, more precise determination of relic abundance and scattering cross-section can be used for obtaining stronger bounds on the allowed parameter space of this kind of model.

Acknowledgements

We would like to thank Joydeep Chakraborty, Partha Konar and Subhendra Mohanty for most useful comments and discussions and for their help in improving the draft.

Appendices

A. CALCULATION OF $w(s)$

Let ϕ be the scattering angle between incoming DM particles then $w(s)$ can be defined as

$$w(s) = \frac{1}{32\pi} \sqrt{\frac{s - 4m_{final}^2}{s}} \int \frac{d\cos\phi}{2} \sum_{\text{all possible channels}} |\mathcal{M}|^2. \quad (28)$$

The function $|\mathcal{M}|^2$ contains not only interaction part, but also contains the kinematical part. Considering the processes as in eq. (18) we can write

$$\begin{aligned} w(s)_{b,\tau,W,Z} = & \left[\frac{\sin^2\alpha \cos^2\alpha}{4} \left(4y_{n_3}^2 (s - 4m_{N_R^3}^2) \right) \right] \times \\ & \left[\frac{1}{(s - m_h^2)^2 + \Gamma_h^2 m_h^2} + \frac{1}{(s - m_H^2)^2 + \Gamma_H^2 m_H^2} \right. \\ & \left. - 2 \frac{(s - m_h^2)(s - m_H^2) + m_h m_H \Gamma_h \Gamma_H}{((s - m_h^2)^2 + \Gamma_h^2 m_h^2)((s - m_H^2)^2 + \Gamma_H^2 m_H^2)} \right] \times \\ & \left[\left\{ \frac{1}{8\pi} \sqrt{\frac{s - m_b^2}{s}} 4y_b^2 \left(\frac{s}{4} - m_b^2 \right) 3 \right\} + \left\{ \frac{1}{8\pi} \sqrt{\frac{s - m_\tau^2}{s}} 4y_\tau^2 \left(\frac{s}{4} - m_\tau^2 \right) \right\} \right. \\ & + \left\{ \frac{1}{8\pi} \sqrt{\frac{s - m_W^2}{s}} \left(\frac{2m_W^2}{v} \left(s + \frac{1}{2m_W^4} \left(\frac{s}{2} - m_W^2 \right) \right) \right) \right\} \\ & \left. + \left\{ \frac{1}{8\pi} \sqrt{\frac{s - m_Z^2}{s}} \left(\frac{m_Z^2}{v} \left(s + \frac{1}{2m_Z^4} \left(\frac{s}{2} - m_Z^2 \right) \right) \right) \right\} \right]. \quad (29) \end{aligned}$$

In this expression second line is the propagator function which includes both h and H . Third line shows decay cross section to $b\bar{b}$ and $\tau^+\tau^-$, whereas, fourth and fifth line is decay cross section to W^+W^- and ZZ respectively. In addition, we have also considered the annihilation into the SM-like Higgs bosons, for which $w(s)_h$ is given by,

$$w(s)_h = \left\{ \frac{1}{16\pi} \left[4y_{n_3}^2 (s - 4m_{N_R^3}^2) \right] \sqrt{\frac{s - m_h^2}{s}} \right. \\ \left. \left(\left(\frac{\sin\alpha}{\sqrt{2}} \right)^2 \frac{\lambda_{hhh}^2}{(s - m_h^2)^2 + \Gamma_h^2 m_h^2} + \left(\frac{\cos\alpha}{\sqrt{2}} \right)^2 \frac{\lambda_{Hhh}^2}{(s - m_H^2)^2 + \Gamma_H^2 m_H^2} \right. \right. \\ \left. \left. - \frac{\sin\alpha \cos\alpha \lambda_{hhh} \lambda_{Hhh} \{(s - m_h^2)(s - m_H^2) + m_h m_H \Gamma_h \Gamma_H\}}{((s - m_h^2)^2 + \Gamma_h^2 m_h^2) ((s - m_H^2)^2 + \Gamma_H^2 m_H^2)} \right) \right\}, \quad (30)$$

where, λ_{hhh} and λ_{Hhh} are calculated by expanding the Higgs potential part,

$$\begin{aligned} \lambda_{hhH} &= 3\lambda_1 v (\cos^2\alpha \sin\alpha) + 3\lambda_2 v_{\text{B-L}} (\cos\alpha \sin^2\alpha) \\ &\quad + \frac{1}{8}\lambda_3 \{ v_{\text{B-L}} (\cos\alpha + 3\cos(3\alpha)) + v (\sin\alpha - 3\sin(3\alpha)) \}, \\ \lambda_{hhh} &= \frac{\lambda_1}{4} v (3\cos\alpha + \cos(3\alpha)) + \frac{\lambda_2}{4} v_{\text{B-L}} (-3\sin\alpha + \sin(3\alpha)) \\ &\quad + \frac{\lambda_3}{8} \{ v (\cos\alpha - \cos(3\alpha)) - v_{\text{B-L}} (\sin\alpha + \sin(3\alpha)) \}. \end{aligned} \quad (31)$$

Finally, $w(s) = w(s)_{b,\tau,W,Z} + w(s)_h$.

B. LOOP FUNCTIONS INVOLVED IN $\langle\sigma v\rangle_{\gamma\gamma}$

The loop functions involved in Higgs to di-photon process are depicted as:

$$\begin{aligned} F_t(\tau) &= -2\tau[1 + (1 - \tau)f(\tau)], \\ F_W(\tau) &= 2 + 3\tau + 3\tau(2 - \tau)f(\tau), \end{aligned}$$

and

$$f(\tau) = \begin{cases} \left(\sin^{-1} \sqrt{1/\tau} \right)^2, & \text{for } \tau \geq 1 \\ -\frac{1}{4} \left(\ln \frac{1 + \sqrt{1-\tau}}{1 - \sqrt{1-\tau}} - i\pi \right)^2 & \text{for } \tau < 1. \end{cases}$$

For, $m_h = 125$ GeV the loop-functions becomes,

$$F_t(\tau_t) = 1.83, \quad F_W(\tau_W) = -8.32.$$

C. CALCULATION FOR DECAY WIDTH OF HEAVY SCALAR

In this model we have two Higgs mass eigenstates (h, H) which are admixture of the gauge eigenstates with the mixing angle α . The SM gauge eigenstate (ϕ) can be written as

$$\phi = \cos\alpha h + \sin\alpha H.$$

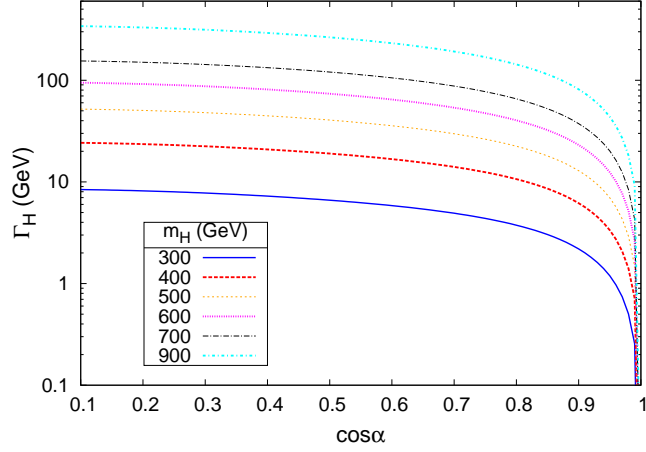


FIG. 6: Plot of heavy scalar boson decay width as a function of scalar mixing angle $\cos\alpha$ for different values of m_H .

So the coupling of $h(H)$ with the SM particles will be multiplied by $\cos\alpha(\sin\alpha)$.

Decay of heavy scalar into fermion–antifermion (SM) pair

$$\Gamma(H \rightarrow f\bar{f}) = N_c \frac{g^2 m_f^2 m_H}{32 \pi m_W^2} \left\{ 1 - \frac{4m_f^2}{m_H^2} \right\}^{3/2} (\sin\alpha)^2 \quad (32)$$

where N_c is color factor, 1 for leptons and 3 for quarks.

Decay of heavy scalar into W boson pair

$$\Gamma(H \rightarrow W^+W^-) = \frac{g^2 m_H^3}{64 \pi m_W^2} \sqrt{1 - \frac{4m_W^2}{m_H^2}} \left[1 - \frac{4m_W^2}{m_H^2} + \frac{3}{4} \left(\frac{4m_W^2}{m_H^2} \right)^2 \right] (\sin\alpha)^2 \quad (33)$$

Decay of heavy scalar into Z boson pair

$$\Gamma(H \rightarrow ZZ) = \frac{g^2 m_H^3}{128 \pi m_W^2} \sqrt{1 - \frac{4m_Z^2}{m_H^2}} \left[1 - \frac{4m_Z^2}{m_H^2} + \frac{3}{4} \left(\frac{4m_Z^2}{m_H^2} \right)^2 \right] (\sin\alpha)^2 \quad (34)$$

Decay of heavy scalar into RH neutrinos

$$\Gamma(H \rightarrow N_R N_R) = \frac{m_{N_R}^2 m_H}{16 \pi v_{B-L}^2} \left(1 - \frac{4m_{N_R}^2}{m_H^2} \right)^{3/2} (\cos\alpha)^2 \quad (35)$$

Decay of heavy scalar into the SM like Higgs

$$\Gamma(H \rightarrow hh) = \frac{\lambda_{Hhh}^2}{32 \pi m_H} \sqrt{1 - \frac{4m_h^2}{m_H^2}} \quad (36)$$

Figure. 6 shows the dependence of total decay width of the heavy scalar boson Γ_H^{tot} on the scalar mixing $\cos\alpha$ for different values of m_H . For higher m_H , the decay-width becomes larger for large mixing. This plot also shows that for the limiting case when $\cos\alpha \rightarrow 1.0$, i.e, without mixing between the scalar bosons, $\Gamma_H^{tot} \rightarrow 0$ and hence it is completely de-coupled from the SM.

-
- [1] G. Hinshaw et al. Nine-Year Wilkinson Microwave Anisotropy Probe (WMAP) Observations: Cosmological Parameter Results. 2012.
 - [2] P.A.R. Ade et al. Planck 2013 results. XVI. Cosmological parameters. 2013.
 - [3] Yoshiaki Sofue and Vera Rubin. Rotation curves of spiral galaxies. *Ann.Rev.Astron.Astrophys.*, 39:137–174, 2001.
 - [4] Douglas Clowe, Marusa Bradac, Anthony H. Gonzalez, Maxim Markevitch, Scott W. Randall, et al. A direct empirical proof of the existence of dark matter. *Astrophys.J.*, 648:L109–L113, 2006.
 - [5] Matthias Bartelmann. Gravitational Lensing. *Class.Quant.Grav.*, 27:233001, 2010.
 - [6] R. Benton Metcalf, Leonidas A. Moustakas, Andrew J. Bunker, and Ian R. Parry. Spectroscopic gravitational lensing and limits on the dark matter substructure in Q2237+0305. *Astrophys.J.*, 607:43–59, 2004.
 - [7] Gerard Jungman, Marc Kamionkowski, and Kim Griest. Supersymmetric dark matter. *Phys.Rept.*, 267:195–373, 1996.
 - [8] Gianfranco Bertone, Dan Hooper, and Joseph Silk. Particle dark matter: Evidence, candidates and constraints. *Phys.Rept.*, 405:279–390, 2005.
 - [9] Lars Bergstrom. Dark Matter Candidates. *New J.Phys.*, 11:105006, 2009.
 - [10] John McDonald. Gauge singlet scalars as cold dark matter. *Phys.Rev.*, D50:3637–3649, 1994.
 - [11] C.P. Burgess, Maxim Pospelov, and Tonnis ter Veldhuis. The Minimal model of nonbaryonic dark matter: A Singlet scalar. *Nucl.Phys.*, B619:709–728, 2001.
 - [12] Hooman Davoudiasl, Ryuichiro Kitano, Tianjun Li, and Hitoshi Murayama. The New minimal standard model. *Phys.Lett.*, B609:117–123, 2005.
 - [13] Wan-Lei Guo and Yue-Liang Wu. The Real singlet scalar dark matter model. *JHEP*, 1010:083, 2010.
 - [14] Abhijit Bandyopadhyay, Sovan Chakraborty, Ambar Ghosal, and Debasish Majumdar. Constraining Scalar Singlet Dark Matter with CDMS, XENON and DAMA and Prediction for Direct Detection Rates. *JHEP*, 1011:065, 2010.
 - [15] James M. Cline, Kimmo Kainulainen, Pat Scott, and Christoph Weniger. Update on scalar singlet dark matter. 2013.

- [16] Yeong Gyun Kim, Kang Young Lee, and Seodong Shin. Singlet fermionic dark matter. *JHEP*, 0805:100, 2008.
- [17] Seungwon Baek, P. Ko, Wan-Il Park, and Eibun Senaha. Vacuum structure and stability of a singlet fermion dark matter model with a singlet scalar messenger. *JHEP*, 1211:116, 2012.
- [18] M.M. Ettefaghi and R. Moazzemi. Annihilation of singlet fermionic dark matter into two photons. *JCAP*, 1302:048, 2013.
- [19] Shinya Kanemura, Takehiro Nabeshima, and Hiroaki Sugiyama. TeV-Scale Seesaw with Loop-Induced Dirac Mass Term and Dark Matter from $U(1)_{B-L}$ Gauge Symmetry Breaking. *Phys.Rev.*, D85:033004, 2012.
- [20] Hiroshi Okada and Takashi Toma. Fermionic Dark Matter in Radiative Inverse Seesaw Model with $U(1)_{B-L}$. *Phys.Rev.*, D86:033011, 2012.
- [21] Yuji Kajiyama, Hiroshi Okada, and Takashi Toma. Light Dark Matter Candidate in B-L Gauged Radiative Inverse Seesaw. *Eur.Phys.J.*, C73:2381, 2013.
- [22] Ernest Ma. Verifiable radiative seesaw mechanism of neutrino mass and dark matter. *Phys. Rev. D*, 73:077301, Apr 2006.
- [23] Nobuchika Okada and Osamu Seto. Higgs portal dark matter in the minimal gauged $U(1)_{B-L}$ model. *Phys.Rev.*, D82:023507, 2010.
- [24] Shinya Kanemura, Osamu Seto, and Takashi Shimomura. Masses of dark matter and neutrino from TeV scale spontaneous $U(1)_{B-L}$ breaking. *Phys.Rev.*, D84:016004, 2011.
- [25] Nobuchika Okada and Yuta Orikasa. Dark matter in the classically conformal B-L model. *Phys.Rev.*, D85:115006, 2012.
- [26] Shaaban Khalil. Low scale $B - L$ extension of the Standard Model at the LHC. *J.Phys.*, G35:055001, 2008.
- [27] Lorenzo Basso, Stefano Moretti, and Giovanni Marco Pruna. A Renormalisation Group Equation Study of the Scalar Sector of the Minimal B-L Extension of the Standard Model. *Phys.Rev.*, D82:055018, 2010.
- [28] Lorenzo Basso. Phenomenology of the minimal B-L extension of the Standard Model at the LHC. 2011.
- [29] E. Aprile et al. Dark Matter Results from 225 Live Days of XENON100 Data. *Phys.Rev.Lett.*, 109:181301, 2012.
- [30] Luca Scotto Lavina. Latest results from XENON100 data. 2013.
- [31] D.S. Akerib et al. First results from the LUX dark matter experiment at the Sanford Underground Research Facility. 2013.
- [32] Elena Aprile. The XENON1T Dark Matter Search Experiment. 2012.
- [33] A.A. Abdo, M. Ackermann, M. Ajello, W.B. Atwood, L. Baldini, et al. Fermi LAT Search for Photon Lines from 30 to 200 GeV and Dark Matter Implications. *Phys.Rev.Lett.*, 104:091302, 2010.
- [34] J. Beringer et al. Review of particle physics. *Phys. Rev. D*, 86:010001, Jul 2012.
- [35] Edward W. Kolb and Michael S. Turner. The Early universe. *Front.Phys.*, 69:1–547, 1990.
- [36] Mark Srednicki, Richard Watkins, and Keith A. Olive. Calculations of Relic Densities in the Early

- Universe. *Nucl.Phys.*, B310:693, 1988.
- [37] John R. Ellis, Andrew Ferstl, and Keith A. Olive. Reevaluation of the elastic scattering of supersymmetric dark matter. *Phys.Lett.*, B481:304–314, 2000.
- [38] John F. Gunion, Howard E. Haber, Gordon L. Kane, and Sally Dawson. THE HIGGS HUNTER’S GUIDE. *Front.Phys.*, 80:1–448, 2000.
- [39] Abdelhak Djouadi. The Anatomy of electro-weak symmetry breaking. I: The Higgs boson in the standard model. *Phys.Rept.*, 457:1–216, 2008.
- [40] M. Ackermann et al. Fermi LAT Search for Dark Matter in Gamma-ray Lines and the Inclusive Photon Spectrum. *Phys.Rev.*, D86:022002, 2012.
- [41] Torsten Bringmann, Xiaoyuan Huang, Alejandro Ibarra, Stefan Vogl, and Christoph Weniger. Fermi LAT Search for Internal Bremsstrahlung Signatures from Dark Matter Annihilation. *JCAP*, 1207:054, 2012.
- [42] Christoph Weniger. A Tentative Gamma-Ray Line from Dark Matter Annihilation at the Fermi Large Area Telescope. *JCAP*, 1208:007, 2012.
- [43] Torsten Bringmann and Christoph Weniger. Gamma Ray Signals from Dark Matter: Concepts, Status and Prospects. *Phys.Dark Univ.*, 1:194–217, 2012.